Bayesian-Inference-based Inverse Estimation of Small Angle Scattering

Akinori Asahara,[1] **Hidekazu Morita,**[1] **Masao Yano,**[2] **Tetsuya Shoji,**[2]
Kanta Ono[3]**, Chiharu Mitsumata**[4]**, Kotaro Saito**[5]

[1]Hitachi Ltd., [2]Toyota Motor Corporation, [3]High Energy Accelerator Research Organization
[4]National Institute for Materials Science, [5]Paul Scherrer Institute

Abstract

As an application of machine-learning algorithms, we improved SAS (Small Angle Scattering), which is common experiment in material science, by developing a Bayesian inference and deriving the confidence-level contour. In the SAS experiment, the grain-size of the sample material has to be estimated from the distribution of the scattered beam. A stochastic model and maximum-likelihood inference with EM-algorithm are often used, but the result is noisy due to data noise. With the proposed method, the grain-size distribution can be estimated similarly to the maximum-likelihood inference method and the confidence levels can be visualized. Thus, researchers can determine estimation reliability and decide whether there are sufficient data. Simulation-generated datasets were processed with the proposed method to evaluate its effectiveness, and it was confirmed that it is useful for automatic SAS data analysis.

Introduction

Information technology for making material development faster, sometimes called Materials Informatics (MI), being investigated(National Institute of Standards and Technology 2019). This technology will help researchers to extract new knowledge of materials.

One of the usecases of the technology is to automatically find features of new materials characteristics from experimental data. Traditionally, researchers carefully inspected experimental data to find such features. However, it is time-consuming and the researchers might miss such features. To solve this problem, methods known as "data mining" are applicable to finding such features. With these methods, knowledge extraction from experimental data can be carried out automatically. Therefore, experiments are made faster.

This paper focuses on small-angle scattering (SAS) (Higgins and Benoît 1994)(Asahara et al. 2019). SAS is a scattering experiment for observing the microstructures of materials. In this experiment, the particle beam incident upon the sample interacts with the microstructures inside. An instrument setting of SAS is illustrated in Fig. 1. The directions of the particles change due to interactions with the microstructures of the materials. The number of particle de-
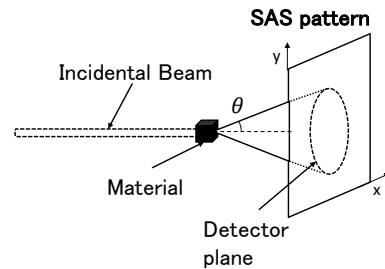
Figure 1: SAS Experiment

tection events on a plane during SAS form a pattern on the plane (called an SAS pattern), reflecting the features of the microstructures. Various particles, such as those of x-ray, ion-beam, etc, can be applied to SAS.

One of the objectives of SAS is estimation of microscale-grain-size distribution in material samples. Material science researchers carefully observe SAS patterns to obtain grain-size information about the microstructure of the sample material.

Therefore, several automatic estimation methods of grain-size distribution with SAS pattern data have been proposed. One of the such methods, called Indirect Fourier Transformation (IFT), is a based on function optimization to fit the grain-size distribution to SAS pattern. However that requires lots of effort for parameter adjustment by material science researchers. To reduce such effort, a maximum-likelihood (ML) inference (Asahara et al. 2020), is a stochastic method for machine learnings, was proposed. The ML inference frees researchers from such effort due to the probabilistic modeling of SAS experimental processes but its reliability is insufficient. ML inference tends to fit to the noise caused by observation because it is point-wise, that is, the result is only one certain parameter setting.

A method of Bayesian inference and a derivation of the confidence level contour are proposed in this work. For Bayesian inference, parameters of the model for SAS are also stochastic, i.e., the probabilities of certain grain-size distributions can be evaluated when an SAS pattern is obtained. Because all grain-size distributions derived from the proposed method can be reliably considered as possible solutions, the contour with a confidence level higher than the
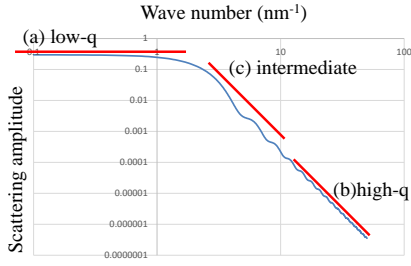
Figure 2: SAS pattern analysis with graphs

given threshold can be visualized.

Problem Settings

Small Angle Scattering

In SAS, particle beam incident upon the sample interacts with the microstructures inside. The directions of the particles thus change due to the interactions. The angle θ between a straight beam and the changed direction of the scattered beam depends on the interaction. Finally, detectors arranged on a plane detect the scattered beam. The number of detection events form SAS pattern on the plane.

The particle behavior during SAS is stochastic, modeled with a differential equation known as the Schödinger equation. Because the distance between the sample and plane is large enough, the coordinate values on the plane $\mathbf{x} = (x, y)$ are approximately in proportion to θ. The probability density function (PDF) $P(\mathbf{x})$ of detection corresponds to the probability that a particle goes in the direction of θ, which is related to microscopic structures called grains.

Assume a simple case in which the grains are balls. Intensity $I(r, q)$ of an SAS pattern scattered with balls of radius r (grain size) is proportional to $\mathcal{I}(r, q)$ as follows,

$$I(r, q) \propto \mathcal{I}(r, q) = \frac{1}{r^3} \left(\frac{\sin qr}{q^3} - \frac{r \cos qr}{q^2} \right)^2, \quad (1)$$

where the q indicates a quantity called wave number, which is the frequency of the wave function multiplied by 2π. The frequency of the wave function is three dimensional because it is derived with the Fourier transformation of the wave function in three dimensional space. The θ depends on the frequency, so the size of $q = \mathbf{q}$ along the vertical vector to the incident beam ("$\mathbf{q} = (q_x, q_y)$" in Fig 1) appears in the formula. Therefore, q indicates the location $\mathbf{x}$ on the detection plane, derived from distance between the incident beam center and that location. That is, we can obtain actual SAS intensity corresponding to $I(r, q)$ by converting $\mathbf{x}$ to q.

An SAS pattern formed by multiple grain sizes is the weighted sum of $\mathcal{I}(r, q)$ over r, and the weight is the grain-size distribution $f(r)$ of the material. Accordingly the scattering pattern $S(q)$ is derived as

$$S(q) \propto \int f(r) I(r, q) \mathrm{d}r. \quad (2)$$

To estimate $f(r)$, $S(q)$, which is the integration of $f(r)I(r, q)$, should be decomposed to the summation of

$I(r, q)$; however, this is difficult, relating to the phase problem(Feigin, Svergun et al. 1987). Thus, material science researchers have tried to guess $f(r)$ with clues from small features latent in the plot of $\mathcal{I}(r, q)$, as shown in Fig. 2. This figure presents a log-log plot of an SAS pattern, and its domain is separated into three parts (a), (b), and (c). In (a) ($q \to 0$) and (b) ($q \to \infty$) , $S(q)$ behaves linearly, being independent from r as shown the graph. Only in (c), $\mathcal{I}(r, q)$ oscillates and it's frequency depends on r. Material science researchers accordingly have to discover the fluctuation at (c) because it gives implicit hints to determine $f(r)$. Therefore, $f(r)$ is only roughly estimated. If $f(r)$ is estimated directly, the SAS could provide much more information of the sample.

Threfore, a method for automatic estimation of $f(r)$ is needed.

Related Works

Indirect Fourier Transformation

Parametric function fitting is a known automatic grain-size estimation method for SAS. With this method, parameters of the function $f(r)$ are adjusted to fit to the obtained SAS pattern(Joachim and Ingo 2018). However, the form of $f(r)$ is required and the true $f(r)$ is generally unknown in actual situations.

To avoid such difficulty, a function having a more general formula should be used. One method using such a function is Indirect Fourier Transform (IFT) (Otto 1977). With IFT, weighted summation of multiple stepwise functions $\theta_n(x)$, where $\theta_n(r)$ returns 1 when $r_n < r < r_{n+1}$, and 0 otherwise, is assumed as the formula. The integral of $S(q)$ under this assumption is decomposed into definite integrations which can be carried out analytically and reformed as a linear combination of the weights, denoted a_n. After minimizing the difference between the linear combination of a_n and the SAS pattern, $f(r)$ is obtained as the sum of $a_n \theta_n(r)$.

The resolution of $f(r)$ is determined by θ_n with IFT, as shown above. Therefore, the range of θ_n should be small to improve the resolution of $f(r)$. However the higher resolution setting makes estimation error larger because more a_ns have to be determined when the range of θ_n is set smaller. The SAS pattern must be more accurate because the number of detection events in the small range are few and sensitive to small errors.

A method for avoiding this problem is to add regularization terms to suppress over fitting. However, the regularization terms must be adjusted manually. To automate regularization, complicated methods for determining the regularization terms have been proposed, but they are not in wide use yet.

Maximum Likelihood Inference

Another method is ML inference, often used for machine learning. The SAS process is modeled as a stochastic process with latent variables which indicates the r of particle interaction. The likelihood derived from the stochastic process is maximized to fit the SAS pattern. As a result, (r) is obtained as the optimal model parameter of the stochastic
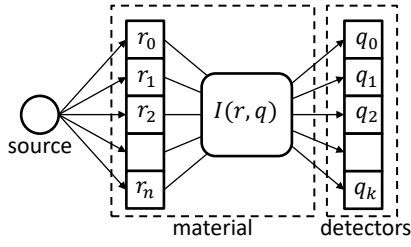
Figure 3: Probabilistic solution of scattering problems

process. No assumption is required for this method if a non-parametric model (that is, a very general stochastic model such as a Gaussian mixture) is applied for the SAS process.

The expectaion-maximizedion (EM) algorithm(Bishop 2006) is a well known algorithm for non-parametric ML inference (Zhang 1993)(Demoment 1989) (Nagata, Sugita, and Okada 2012). Similar methods are used in astrophysics (William 1972) (Leon 1974), bioinformatics (Lustig et al. 2008) (Lustig, Donoho, and Pauly 2007) and compressed sensing (Donoho 2006). An application for grain-size estimation was also proposed(Asahara et al. 2020). The SAS process is modeled as a combination of two random choice processes for the EM algorithm. In the first process, the incident beam interacts with grains, and in second process, the incident beam changes its direction and arrives at a point on the detector plane. E-step to obtain the expectation value of interacting grains and M-step to obtain $f(r)$ with ML are iteratively carried out to derive the solution of the ML inference.

The EM algorithm automatically derives $f(r)$, though the result is noisy when a noisy SAS pattern is input. As shown in Formula (1), the rate of event detection at high-q decreases in proportion to $1/q^4$. Thus, a long time to collect detection events is required to obtain the detection events at higher q. An SAS pattern does not reflect probability at high-q when the experimental time is limited. This causes noisy SAS patterns.

Such noise can be reduced by obtaining more detection events; however, the cost is extremely high. Since the generation of incidental particle beam, such as a neutron beam, is costly, researchers have to save on beam time. Therefore estimation reliability should be evaluated, since the experiment should be finished as soon as a sufficient amount of data is obtained.

Proposed Method

MAP Inference

Maximum A Posteriori (MAP) inference is Bayesian parameter estimation method. With MAP inference, a PDF of parameters (called a prior) is defined and revised after obtaining observations (the revised PDF is called a posterior). The parameter setting that gives the maximum posterior is adopted as the inference result. The number of detection events in an SAS pattern is denoted as K integers: $\{n_0, \cdots n_K\}$, where each integer corresponds to the particle detector for each wavenumber. That is, n_k is the number of

detection events at q_k in the SAS pattern. Grain-size parameters to be estimated are as denoted $\{\pi_0, \cdots, \pi_L\}$, where π_i indicates the ratio of r_i grains to all grains and assumed proportional to $f(r)$, which indicates the grain-size ratio. Accordingly, π_i posterior is maximized after obtaining the SAS pattern, which is denoted as $P(\{\pi_i\}|\{n_k\})$.

The $P(\{\pi_i\}|\{n_k\})$ can be easily rewritable with Bayes theorem:

$$P(\{\pi_i\}|\{n_k\}) = \frac{P(\{n_k\}|\{\pi_i\})P(\{\pi_i\})}{P(\{n_k\})}, \quad (3)$$

where $P(\{n_k\})$ is a prior regarding the events related to the wavenumber q_k. Since it is independent from $f(r)$, $P(\{n_k\})$ will be canceled with a normalization constant. Thus the $P(\{n_k\}|\{\pi_i\})$ and the $P(\{\pi_i\})$ should be handled carefully.

The $P(\{n_k\}|\{\pi_i\})$ is the posterior of the number of detection events after determining $\{\pi_i\}$. Note the probability of one-particle detection at q after interaction with r is proportional to $\mathcal{I}(r, q)$ (as shown in (1)). Therefore, the SAS process is modeled as an N-times iteration of the random sampling (the probability is $\sum_i \pi_i I(r_i, q_k)$). That is, $P(\{n_k\}|\{\pi_i\})$ is a multinomial function with the parameter $\sum_i \pi_i I(r_i, q_k)$:

$$P(\{n_k\}|\{\pi_i\}) = \text{Mul}(\{n_k\}; \{\sum_i I(r_i, q_k)\pi_k\}). \quad (4)$$

where $\eta_{jk} = I(q_j, r_k)$ is defined for ease of reference hereafter.

The $P(\{\pi_i\})$ is a prior regarding r. Generally, a prior is determined as the conjugate prior of the posterior (i.e. $P(\{n_k\}|\{\pi_i\})$). Because the conjugate prior of a multinomial distribution is the Dirichlet distribution, the prior of $P(\{n_k\}|\{\pi_i\})$ should be similar to Dirichlet distribution. Accordingly the parameter-transformed the Dirichlet distribution $\hat{\text{Dir}}$ is defined for $P(\{n_k\}|\{\pi_i\})$ as the prior $P(\{\pi_i\})$:

$$P(\{\pi_i\}) = \hat{\text{Dir}}(\{\pi_k\}; \{\alpha_k\}) \propto \prod_K \left(\sum_k \hat{\pi}_l \eta_{lk}\right)^{\alpha_k - 1}, \quad (5)$$

where α_k is a hyperparameter of Dirichlet distribution, which indicates knowlege obtained in advance. This leads to

$$P(\{n_k\}|\{\pi_i\})P(\{\pi_i\})$$
$$= \text{Mul}(\{n_k\}; \{\sum_i \eta_{ik}\pi_k\})\hat{\text{Dir}}(\{\pi_k\}; \{\alpha_k\})$$
$$= \hat{\text{Dir}}(\{\pi_k\}; \{n_k + \alpha_k\}). \quad (6)$$

For estimating $\{\pi_i\}$, $P(\{\pi_i\}|\{n_k\})$ should be maximized with the formulation as $P(\{\pi_i\}|\{n_k\}) \propto P(\{n_k\}|\{\pi_i\})P(\{\pi_i\})$. The procedure to estimate this is similar to that of the EM algorithm. For simplicity, the logarithm of the posterior is maximized by $\{\pi_k\}$ under constraint $\sum \pi_k = 1$. Therefore, the maximization is carried out with the Lagrange multiplier method. Finally, by iterating the following formula until the convergence, $\{\hat{\pi}_l^t\}$ at $t \to \infty$ is obtained as $f(r)$.

$$\hat{\pi}_l^{t+1} = \sum_k \frac{(n_k + \alpha_0)}{\sum(n_k + \alpha_0)} \frac{\hat{\pi}_l^t \eta_{l,k}}{\sum_j \hat{\pi}_j^t \eta_{j,k}}. \quad (7)$$

Algorithm 1: MAP inference of grain size
***
Input: SAS pattern intensity $n_k \geq 0$, wavenumber $q_k \geq 0$
    $(k = 0, 1, \cdots, K)$
    resolution of grain size $r_l \geq 0$ where $(l = 0, 1, \cdots, L)$
Output: $\{\pi_l\}$
    $N \Leftarrow \sum_k (n_k + \alpha_k)$, $\{\eta_{lk}\} \Leftarrow \{\frac{I(r_l, q_k)}{\sum_m I(r_l, q_k)}\}$,
    $\{\pi_l\} \Leftarrow 1/L$
    repeat
        $\{\pi_l\} \Leftarrow \sum_k \frac{n_k + \alpha_k}{N} \frac{\pi_l \eta_{lk}}{\sum_j \pi_j \eta_{jk}}$
    until convergence
***

The algorithm of MAP inference is shown in Algorithm 1.

Uncertainty of Parameters

To evaluate the confidence level of the inference, the accumulation of the probability around the MAP-inference result should be evaluated. The following p_l is the accumulation from the MAP inference result $\hat{\pi}_l$ to $\hat{\pi}_l + \delta$.

$$p_l = \int_{\hat{\pi}_l}^{\hat{\pi}_l + \delta} \mathrm{d}\pi_l \int \int \mathrm{d}\pi_0 \cdots \mathrm{d}\pi_N P(\{\pi_i\} | \{n_{q_k}\}) \quad (8)$$

From this definition, the contour can be visualized with δ determined by p_l, for instance, to visualize the 95% confidence level contour, δ is determined to satisfy $p_l = 0.95$.

To derive δ, the constraint $\sum \pi_l = 1$ should be satisfied during integration. Therefore, integration is difficult to be carried out. For the problem of the difficulty, an approximation is introduced. In $P(\{\pi_i\} | \{n_{q_k}\})$, i.e., the Dirichlet distribution, the effect of $\{\pi_i\}$ changes exponentially. Therefore, the contribution from $\{\pi_i\}$ far from the MAP inference result can be ignored because it decays exponentially.

Consequently π_is are fixed to the following $\tilde{\pi}$, which is near from $\{\hat{\pi}_i\}$, instead of integration.

$$\tilde{\pi}_i = \frac{\hat{\pi}_i}{\sum_{i \neq l} \hat{\pi}_i} \times (1 - (\hat{\pi}_l + \delta)). \quad (9)$$

With the $\tilde{\pi}_i$,

$$p_l \simeq \int_{\hat{\pi}_l}^{\hat{\pi}_l + \delta} P(\tilde{\pi}_0, \cdots, \pi_l \cdots \tilde{\pi}_L | \{n_{q_k}\}) \mathrm{d}\pi_l. \quad (10)$$

The procedure to calculate p_l is simple: iterating π_l is shifted by a very small value, and $P(\tilde{\pi}_0, \cdots, \pi_l \cdots \tilde{\pi}_L | \{n_{q_k}\})$ is added to p_l with recalculated $\tilde{\pi}_i$ until p_l becomes higher than the threshold.

Smoothing, which is used to reduce noise, should be taken into account by the uncertainty calculation. Smoothing to remove noise from the estimation result involves multiply a filter matrix by π_i. A Gaussian filter is often used for this purpose. However, as discussed above, since uncertainty is estimated based on probability, non-stochastic smoothing may make conflicts with the MAP inference result, e.g., negative π_l.

To avoid such conflicts, smoothing should be done with a stochastic model. Remember $\eta_{l,k}$ is multiplied by $\{\pi_i\}$ inside $P(\{\pi_i\} | \{n_{q_k}\})$. Therefore the matrix for smoothing can be merged with $\eta_{l,k}$ as $\sum_j A_{lj} \eta_{l,k}$ where A_{lj} is the smoothing matrix. This change indicates that $\sum_l A_{lj} \pi_l$ not $\{\pi_l\}$ corresponds to r. In this setting, $\{\pi_l\}$ corresponds to the weight of a component such as a Gaussian packet. That is, $f(r)$ is represented as the combination of these components.

Experiments

Experimental Settings

We conducted an experiment to evaluate whether the proposed method can be used to estimate $f(r)$ consistent with an SAS pattern. In the experiment, simulation-generated SAS pattern datasets were processed to compare the results with the ground truth.

The datasets were processed with the proposed method, and ML inference method by the EM algorithm for comparison. Ten thousands iterations of the MAP inference and the EM algorithm were carried out instead of checking convergence, to simulate the situation in which the processing time is limited during the SAS experiment. For the proposed method, a Gaussian-smoothing matrix is multiplied by $\eta_{l,k}$; therefore, the result was expected to be smooth and the confidence level contour to be consistent with it.

In the experiment, three types of diffrent $f(r)$ were defined. Each pattern is one gamma distribution or the sum of three Gamma distributions having the most frequent point around 10nm. The $f(r)$ was discretized by 0.05 nm, and its domain is set from 0 to 20 nm (i.e., 400 values), corresponding to $f(r)$ in (2).

To obtain the SAS patterns, random sampling was carried out. The detection-event number was set to 10,000, and the SAS patterns of the $f(r)$s were generated. First, q's domain, which is from $0.1\mathrm{nm}^{-1}$ to $10\mathrm{nm}^{-1}$, was discretized into 200 lots denoted as q_k. The $S(q_k)$ was calculated by evaluating the integration of (2). Random sampling along $S(q_k)$, i.e. the probability of detection, was carried out to simulate particle-detection events and the event number was counted to generate SAS patterns.

A computer with Intel(R) Core(TM) i3-4150 3.50GHz CPU and 11 GB RAM and Cent OS was used for the experiment. The implementation was based on Python 3.6.5, and numpy library (Oliphant 2006) was used to improve the efficiency of the calculation. Each calculation time lasted about 1 minute, which was short enough for carrying out before SAS is finished.

Settings for the proposed method is as follows: α_k, which is a hyperparameter used in the proposed method, was 1.0; Gaussian-smoothing matrix was $A_{ij} = \exp - \frac{1}{2} \left(\frac{r_i - r_j}{0.5} \right)^2$; the threshold of the confidence contour was 95%.

Experimental Results

Figure 4 shows the results. Figure 4 (a) plots the SAS pattern by log-log plot, Fig. 4 (b) plots $f(r)$ estimated with MAP inference, and Fig.4 (c) plots the $f(r)$ estimated with ML inference for comparison. The blue lines in Fig. 4 (a) plot $10000 \times S(q_k)$ and orange points shows SAS pattern generated with the $S(q_k)$; The black lines in Figs. 4 (b) and (c) plot the truth, i.e. the original $f(r)$; the red lines in Figs.
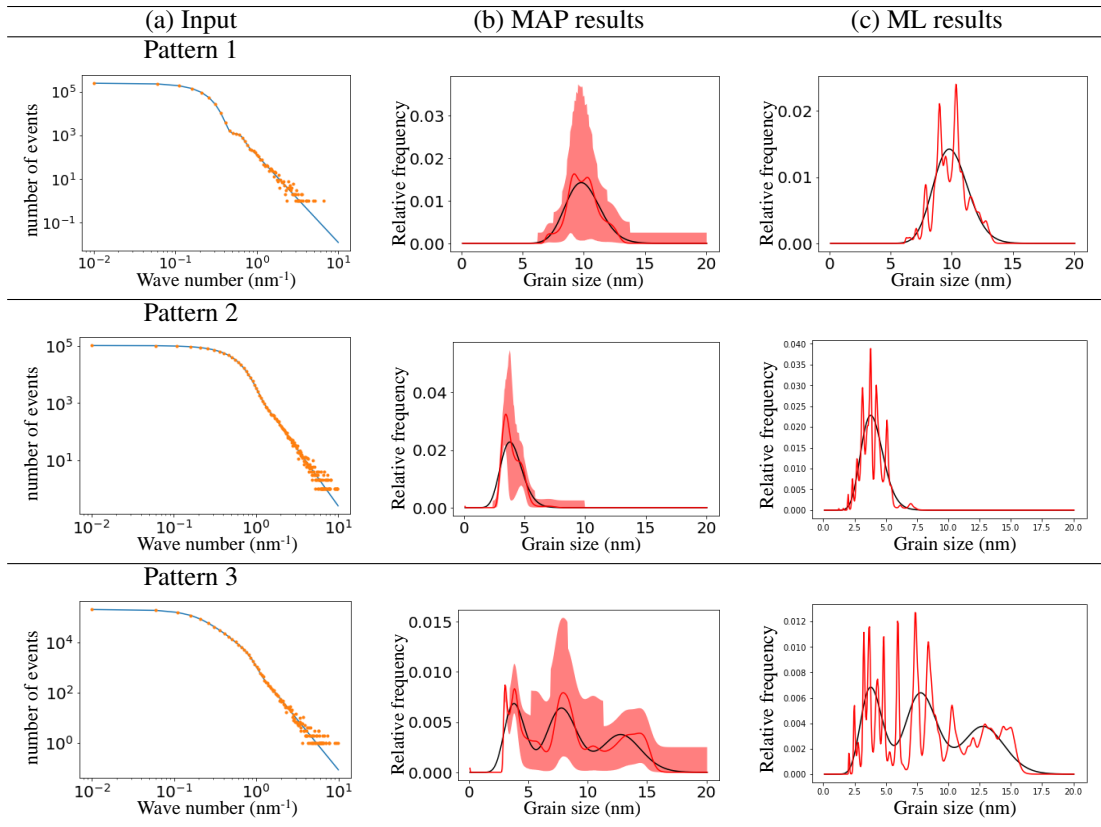
Figure 4: Results of Pattern 1, 2, 3

(b) and (c) plot the estimation results; and red areas indicate 95% confidence.

The $f(r)$ of Pattern 1 has only one peak at the center of the q-range. In Fig. 4 (b), 95% confidence level area indicates that r around the center is quite uncertain. As shown in Fig. 4 (c), the SAS pattern of Pattern 1 is so noisy that the ML inference results become noisy. The MAP inference results are better and the confidence-level area can be drawn without conflicts.

The $f(r)$ of Pattern 2 has a peak at lower q. In Fig. 4 (b), the 95% confidence level area around the peak is extremely high. The MAP inference curve (red curve) differs from the truth curve (black line). However, at low q, the truth curve is outside the 95% confidence level area, showing that the 95% confidence level area is not perfect.

The $f(r)$ of Pattern 3 has three peaks. As shown in Fig. 4 (c), it is difficult to observe the three peaks from the ML inference results. The three peaks from the MAP inference results in Fig. 4 (b) are more readable than those from the ML inference results Fig..4 (c). Though the MAP inference curve differs from the truth curve, most of the truth curve is inside the 95% confidence level area, except for low q.

Discussion

All results in Fig. 4 (b) are similar to tge truth. In contrast, the results in Fig. 4 (c), results include noise. The 95% confidence level area works well, but there are conflicts in low

q. As shown in Fig. 4 (a), the number of events at high q SAS pattern is almost zero or one because $S(q)$ in the high q is very small. The high q corresponds to the low r component of the distribution because the low r corresponds to a large wave number due to $I(q, r)$. Therefore, the results in Fig. 4 (c) oscillate due to the loss of the high-frequency component.

One problem with MAP inference is the behavior at the low-r region. The estimated fluctuation is small in spite of the estimated $f(r)$ being inaccurate. Because $I(r, q)$ is small when both r and q are low, a high q is considered to contribute to this behavior. As mentioned above, the observations at a high q are extremely low. Because sparseness might cause inconsistent visualization, more experiments are required to specify this cause.

Figure 5 shows the results with ML inference when SAS Pattern3 is ideal, i.e. SAS pattern which is completely in proportion to $S(q)$. This shows that the $f(r)$ can be reconstructed if SAS pattern is perfect. Because the low q of Fig. 4 (a) is quite similar to $S(q)$, the difference is considered to ogirin from the high q loss.

Figure 6 shows the results without a Gaussian filter. The confidence level contour is also consistent with the MAP inference results. Similarly to that with the Gaussian filter, the truth is within the 95% confidence level area, except for low r. The results agree but difficult to read due to oscillation. From these results, MAP inference improves the $f(r)$ es-
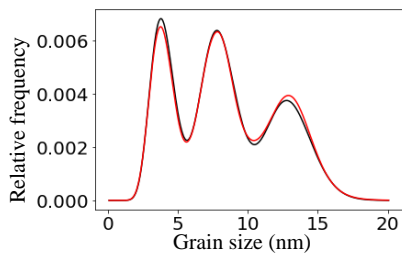
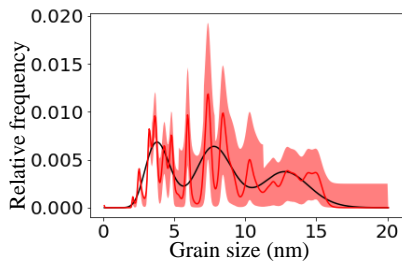Figure 5: ML inference result from ideal SAS pattern

Figure 6: MAP inference results without Gaussian smoother

timation and visualizes it with reliability. This shows that SAS can become more useful for observing the microstructures of materials, except for low r, which indicates grains that are too small to observe during SAS.

Conclusion and Future Work

An MAP inference grain-size-distribution estimation method was proposed for automatically analyzing SAS patterns. The experimental results indicates that the proposed method can accurately estimate the original grain-size distribution from SAS patterns. It enables visualization of parameter fluctuation, whereas ML inference does not. This information will help researchers to decide whether the experimental time is sufficient or not.

For future works, we will attempt to solve the problem with the proposed method. was shown in the experiment, which is inaccurate fluctuation in low r region. We will take it into account non-ball scattering bodies by consideting two dimensional SAS patterns.

References

Asahara, A.; Morita, H.; Mitsumata, C.; Ono, K.; Yano, M.; and Shoji, T. 2019. Early-Stopping of Scattering Pattern Observation with Bayesian Modeling. In *Proceedings of the AAAI Conference on Artificial Intelligence*, volume 33, 9410–9415.

Asahara, A.; Morita, H.; Mitsumata, C.; Ono, K.; Yano, M.; and Shoji, T. 2020. EM-algorithm Enpowers Material Science: Application of Inverse Estimation for Small Angle Scattering. In *Proceedings of the AAAI-MAKE 2020*, volume 2600.

Bishop, C. M. 2006. *Pattern Recognition and Machine Learning*. New York: Springer.

Demoment, G. 1989. Image reconstruction and restoration: overview of common estimation structures and problems. *IEEE Transactions on Acoustics, Speech, and Signal Processing* 37(12): 2024–2036. ISSN 0096-3518. doi: 10.1109/29.45551.

Donoho, D. L. 2006. Compressed sensing. *IEEE Transactions on information theory* 52(4): 1289–1306.

Feigin, L.; Svergun, D. I.; et al. 1987. *Structure analysis by small-angle X-ray and neutron scattering*, volume 1, 25–55. Springer.

Higgins, J. S.; and Benoît, H. 1994. *Polymers and neutron scattering*. Clarendon press Oxford.

Joachim, K.; and Ingo, B. 2018. SASFit. https://www.psi.ch/en/sinq/sansi/sasfit.

Leon, B. L. 1974. An iterative technique for the rectification of observed distributions. *The astronomical journal* 79(6): 745–754.

Lustig, M.; Donoho, D.; and Pauly, J. M. 2007. Sparse MRI: The application of compressed sensing for rapid MR imaging. *Magnetic Resonance in Medicine* 58(6): 1182–1195. ISSN 1522-2594. doi:10.1002/mrm.21391. URL http://dx.doi.org/10.1002/mrm.21391.

Lustig, M.; Donoho, D. L.; Santos, J. M.; and Pauly, J. M. 2008. Compressed Sensing MRI. *IEEE Signal Processing Magazine* 25(2): 72–82. ISSN 1053-5888. doi:10.1109/MSP.2007.914728.

Nagata, K.; Sugita, S.; and Okada, M. 2012. Bayesian spectral deconvolution with the exchange Monte Carlo method. *Neural Networks* 28: 82 – 89. ISSN 0893-6080. doi:http://dx.doi.org/10.1016/j.neunet.2011.12.001. URL http://www.sciencedirect.com/science/article/pii/S0893608011003169.

National Institute of Standards and Technology. 2019. mgi. https://www.nist.gov/mgi(viewed at Oct. 2019).

Oliphant, T. E. 2006. *A guide to NumPy*, volume 1. Trelgol Publishing USA.

Otto, G. 1977. A new method for the evaluation of small-angle scattering data. *Journal of Applied Crystallography* (10): 415–421.

William, Hadley, R. 1972. Bayesian-Based Iterative Method of Image Restoration. *Journal of the Optical Society of America* 62(1): 55–59.

Zhang, J. 1993. The mean field theory in EM procedures for blind Markov random field image restoration. *IEEE Transactions on Image Processing* 2(1): 27–40. ISSN 1057-7149. doi:10.1109/83.210863.